Electronic Supplementary Material (ESI) for Soft Matter.

Supplementary Information

pH Stability and Disassembly Mechanism of Wild-Type Simian Virus 40

Roi Asor[1,2], *Daniel Khaykelson*[1,2], *Orly Ben-nun-Shaul*[3], *Yael Levi-Kalisman*[2,4], *Ariella Oppenheim*[3], and *Uri Raviv*[*1,2]

[1]Institute of Chemistry, The Hebrew university of Jerusalem, Edmond J. Safra Campus, Givat Ram, Jerusalem, 9190401, Israel

[2]Center for Nanoscience and Nanotechnology, The Hebrew University of Jerusalem, Edmond J. Safra Campus, Givat Ram, Jerusalem, 9190401, Israel

[3]Department of Hematology, The Hebrew University-Hadassah Medical School, Ein Kerem, Jerusalem 91120, Israel

[4]Institute of Life Sciences, The Hebrew university of Jerusalem, Edmond J. Safra Campus, Givat Ram, Jerusalem, 9190401, Israel

February 3, 2020

* To whom correspondence should be sent e-mail: uri.raviv@mail.huji.ac.il

1 Additional cryo-TEM images between pH 3 and 10

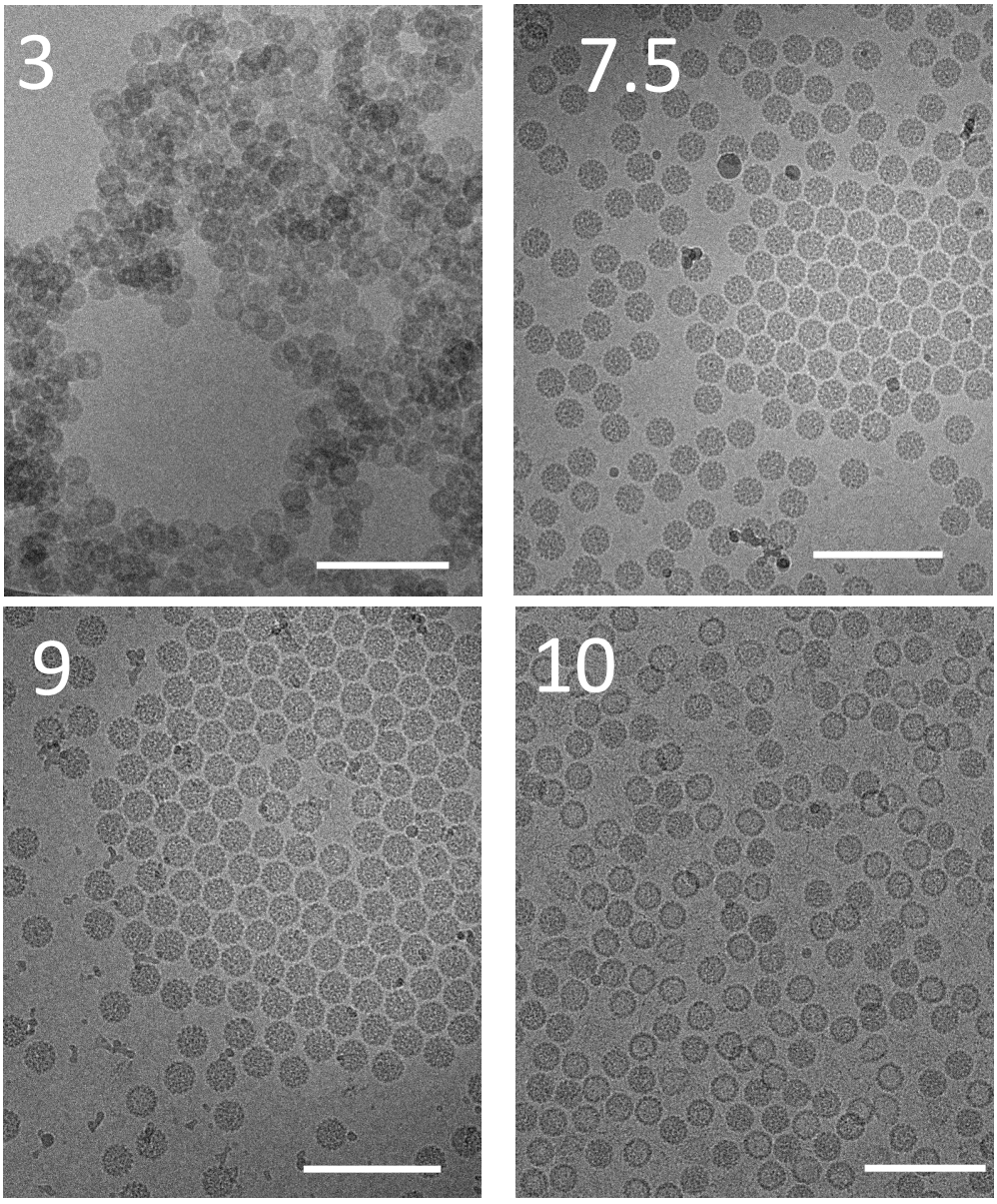

Figure S1: Cryo-TEM images of wtSV40 at different pH values. The pH value is indicated on the upper left corner of each image. At pH 3 capsid aggregates are observed. At pH 10 Full capsids (dark interior) and empty capsids (bright interior) are observed. Scale bars are $200\,\mathrm{nm}$.

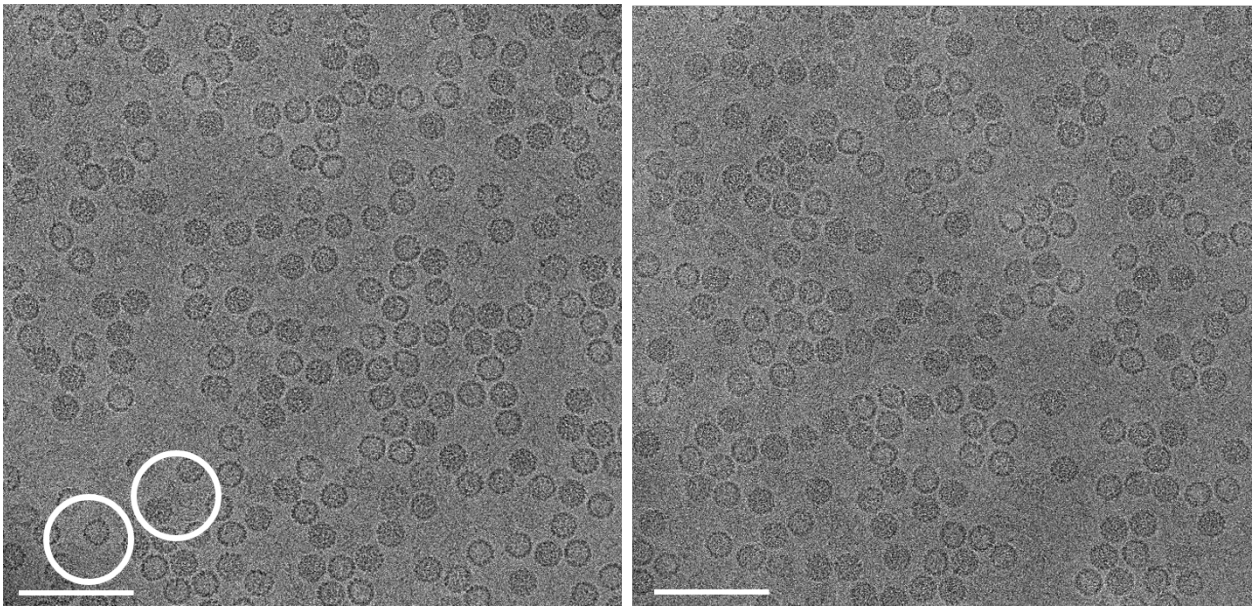

Figure S2: Additional cryo-TEM images of wtSV40 at pH 10. Full and empty capsids are observed as well as DNA which can be seen all over. In the marked virus particles the DNA remained close to the capsid after escaping from the capsid. Scale bars are $200\,\mathrm{nm}$.

2 Cryo-TEM images of empty SV40 particles

The classification of particles seen in the cryo-TEM images as empty or full was done by the change in contrast between the outer capsid wall and the inner volume of the particle. In Figure S3 one can see a reference image containing empty particles extracted from the upper band of the cesium chloride gradient (see Experimental Section). The average density of this band was $\sim$1.3 g/cm^3.

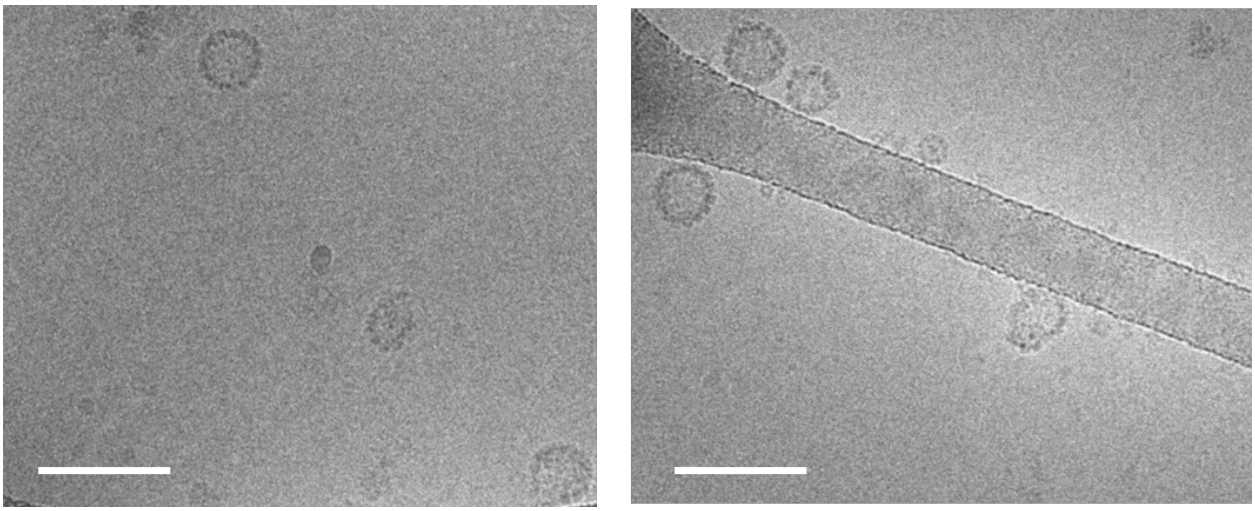

Figure S3: Cryo-TEM images of empty capsids of SV40 in 0.5 M NaCl solution, as reference for the empty capsids observed at pH 10. Scale bars are $100\,\mathrm{nm}$.

3 Fitting the SAXS curve using a model of concentric shells to extract the outer radius of the particles

As shown in Figure 2, wtSV40 remained soluble and stable at pH values between 5.5 and 9. Slight variations, however, were observed in the scattering curves at high pH values. To characterize the change in the dimensions of the virus particles we have fitted the SAXS curves to a low resolution model. At low resolution, the virus electron density contrast ,$\Delta\rho(\vec{r})$, can be approximated as spherical. This assumption holds up to a resolution at which the inter-pentamer correlations significantly contribute to the scattering intensity ($q \sim 0.6\,\mathrm{nm}^{-1}$), as was previously shown[1,2,3]. This approximation, however, is sufficient for determining the outer radius of the particle and to follow the change of the radius in different chemical environments. In Figure 2 the signals were analyzed using low resolution models, computed by X+ software[4,5,6](https://scholars.huji.ac.il/uriraviv/software/x). The analysis was done with a model of concentric spherical shells with a radial electron density profile that was constructed from a sum of hyperbolic tangent functions as explained in our earlier papers[1,5,6]:

$$\Delta\rho\left(r\right)=\sum_{i=1}^{3}\Delta\rho_{i}\left\{\phi\left[\alpha_{i-1}\left(r-R_{i-1}\right)\right]-\phi\left[\alpha_{i}\left(r-R_{i}\right)\right]\right\}, \tag{S1}$$

where

$$\phi\left(r\right)=\frac{\tanh\left(r\right)+1}{2}. \tag{S2}$$

R_i is the outer radius of the i-th layer, $\Delta\rho_i$ is its electron density contrast, and α_i is its slope. The thickness, L_i, of the i-th layer is $L_i = R_i - R_{i-1}$. The model was then fitted to the scattering data by adjusting the thickness and electron density of each layer. Three layers were needed for an adequate fit. The fitting results (Figure S4) and the best fitted parameters (Table S1) are presented here.

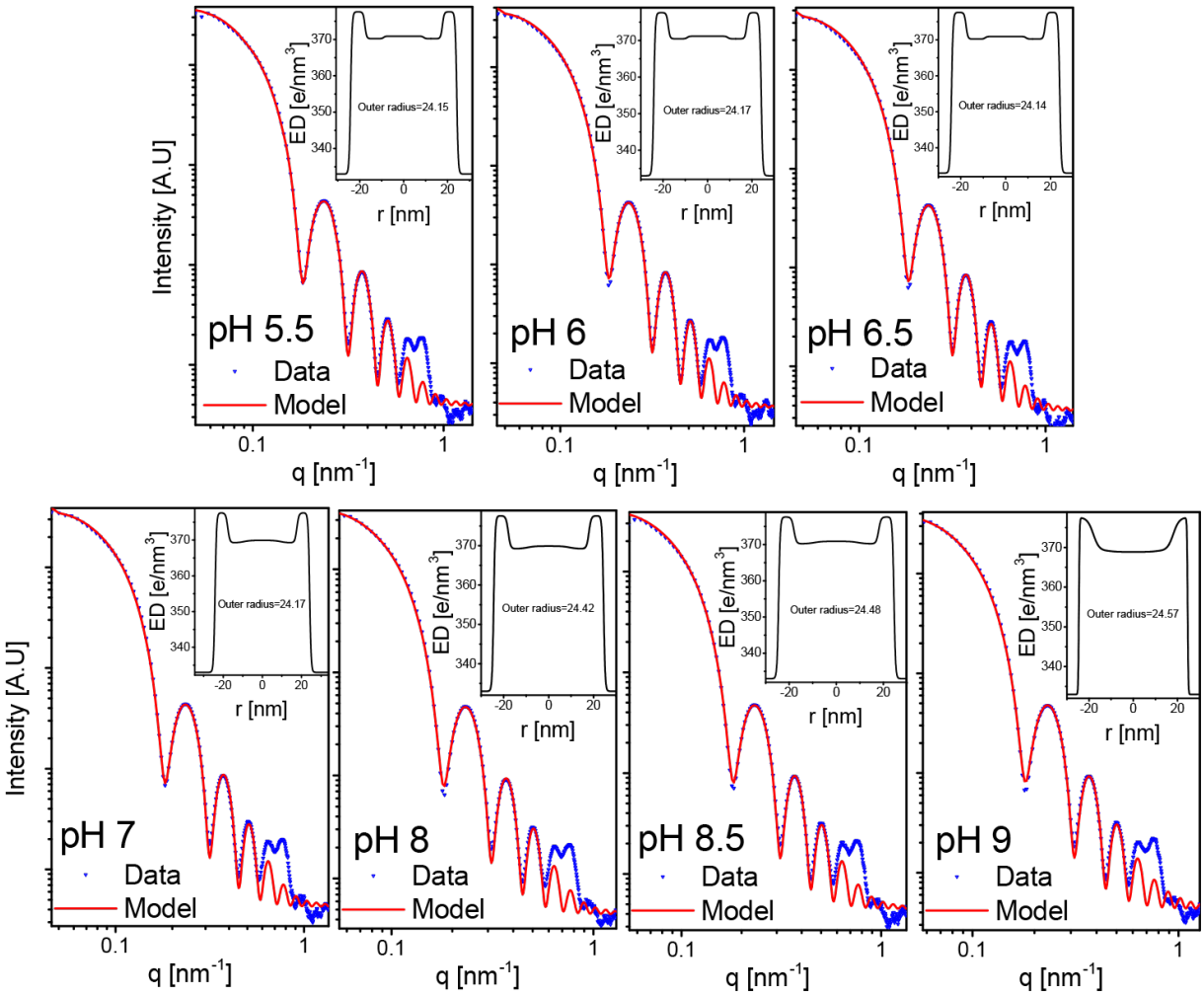

Figure S4: Background subtracted azimuthally averaged SAXS curves from wtSV40 at different pH values (blue symbols, taken from Figure 2). The solid red curves are the fitted models of concentric spherical shells, based on Equation S1. The electron density profiles that best fitted the date are shown at the insets of each pH value. The structural parameters of the three layer structure are given in Table S1.The models were computed and fitted to the data using X+[4,5,6](https://scholars.huji.ac.il/uriraviv/software/x).

The best fitted model parameters are given in Table S1.

Table S1: The fitted electron density profile parameters substituted into Equation S1. R_i is the outer radius of the i-th layer, ρ_i is its electron density, and α_i is its slope (used in Equation S1). The thickness, L_i, of the i-th layer is $L_i \equiv R_i - R_{i-1}$. The electron density contrast is $\Delta\rho_i \equiv \rho_i - \rho_0$, where the solvent electron density, ρ_0, was $333\,{}^{\mathrm{e}}/_{\mathrm{nm}^3}$.

pH	R_3 (Virus outer radius) [nm]	L_1 [nm]	ρ_1 [e/nm^3]	α_1	L_2 [nm]	ρ_2 [e/nm^3]	α_2	L_3 [nm]	ρ_3 [e/nm^3]	α_3
5.5	24.2	9.1	370.9	1.1	8.5	370.2	1.2	6.5	377.6	1.5
6	24.2	9.1	370.9	1.1	8.5	370.2	1.3	6.5	377.6	1.5
6.5	24.1	9.1	370.9	1.1	8.5	370.2	1.3	6.5	377.6	1.5
7	24.2	9.2	369.9	0.3	8.4	369.2	1.0	6.5	377.6	1.3
8	24.4	9.3	369.9	0.3	8.7	369.2	1.0	6.5	377.6	1.5
8.5	24.5	9.3	370.9	0.3	8.7	370.2	1.0	6.5	377.6	1.5
9	24.6	9.5	368.6	1.26	8.6	369.2	0.5	6.5	377.6	1.3

4 Temperature Stability

To test the stability of the particles we measured the scattering intensity of sv40 sampled after short incubation at elevated temperatures. SV40 sample at pH 10 was incubated at 40 °C for a few minutes and then cooled back to 25 °C. As shown in Figure S5 the particles disassembled. At pH 5 however, SV40 particles remained stable even at 55 °C (Figure S6).

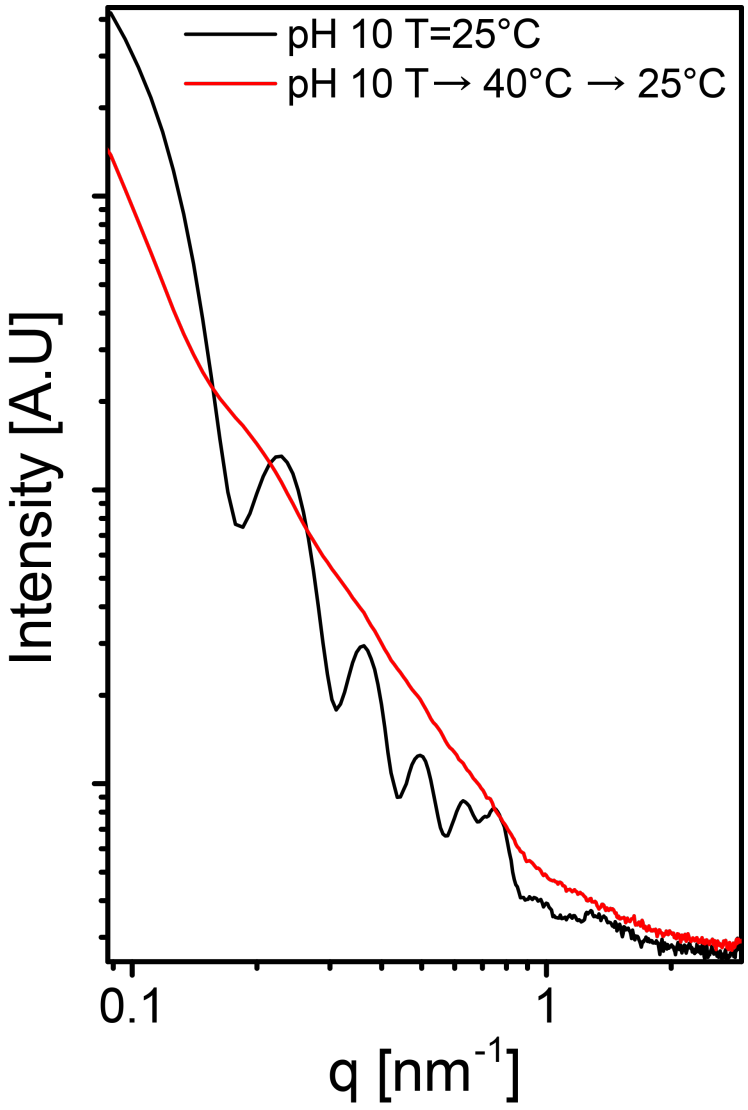

Figure S5: Azimuthally-integrated background-subtracted SAXS curves of wtSV40 in 150 mM NaCl at pH 10 and 25 °C (black curve), and of wtSV40 that was incubated for few minutes at 40 °C and then cooled back to 25 °C (red curve). Date were measured in SWING beamline in Soleil synchrotron.

5 Cryo-TEM of wtSV40 at pH 10.7 using 50 mM CAPS buffer

Figure S7 shows additional cryo-TEM images of wtSV40 at pH 10.7, obtained by using the CAPS buffer. Under those conditions, empty and incomplete capsids coexisted with full particles. The solution also contained the circular dsDNA, the histone octamers, and perntamers (Figure S7b).

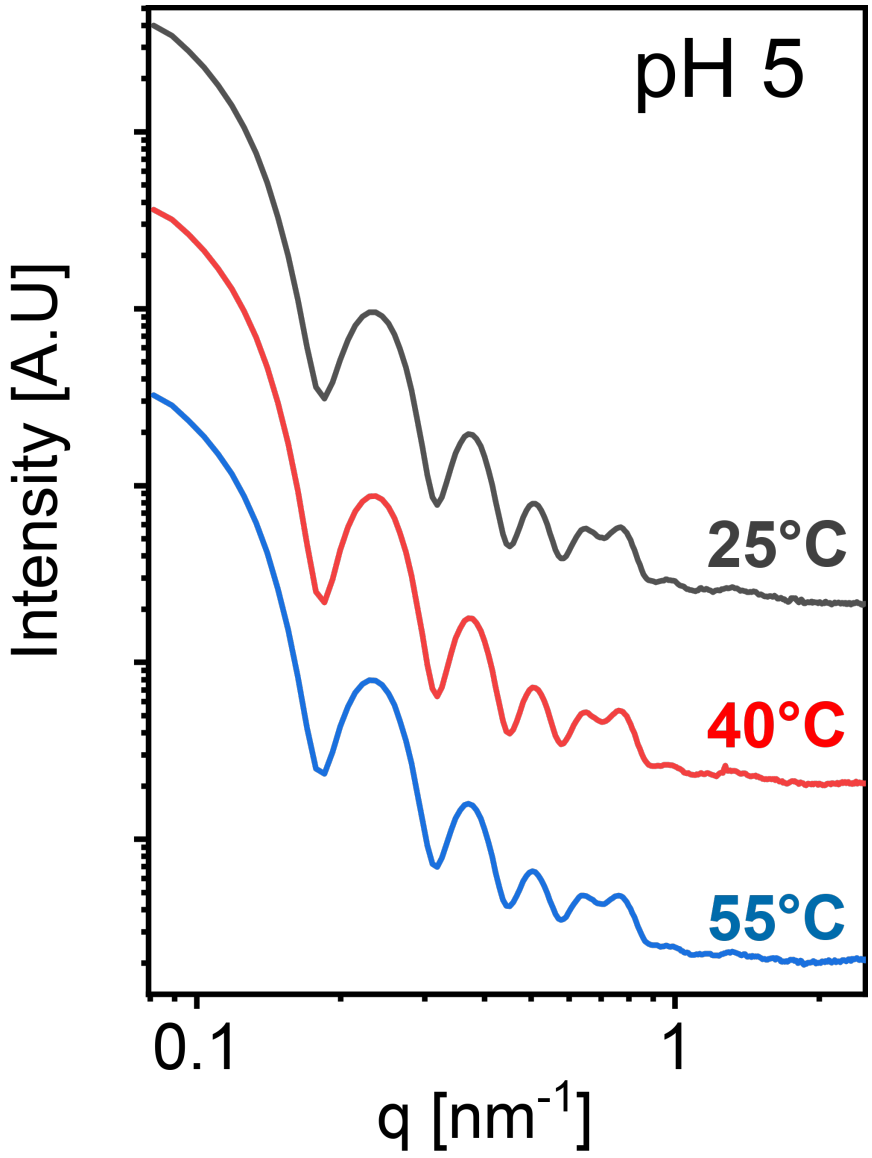

Figure S6: Azimuthally-integrated background-subtracted SAXS curves of wtSV40 in 150 mM NaCl at pH 5 and 25 °C (gray curve), 40 °C (red curve) and 55 °C (blue curve). The samples were incubated for few minutes at each temperature before it was exposed to the X-ray beam. Date were measured in SWING beamline in Soleil synchrotron.

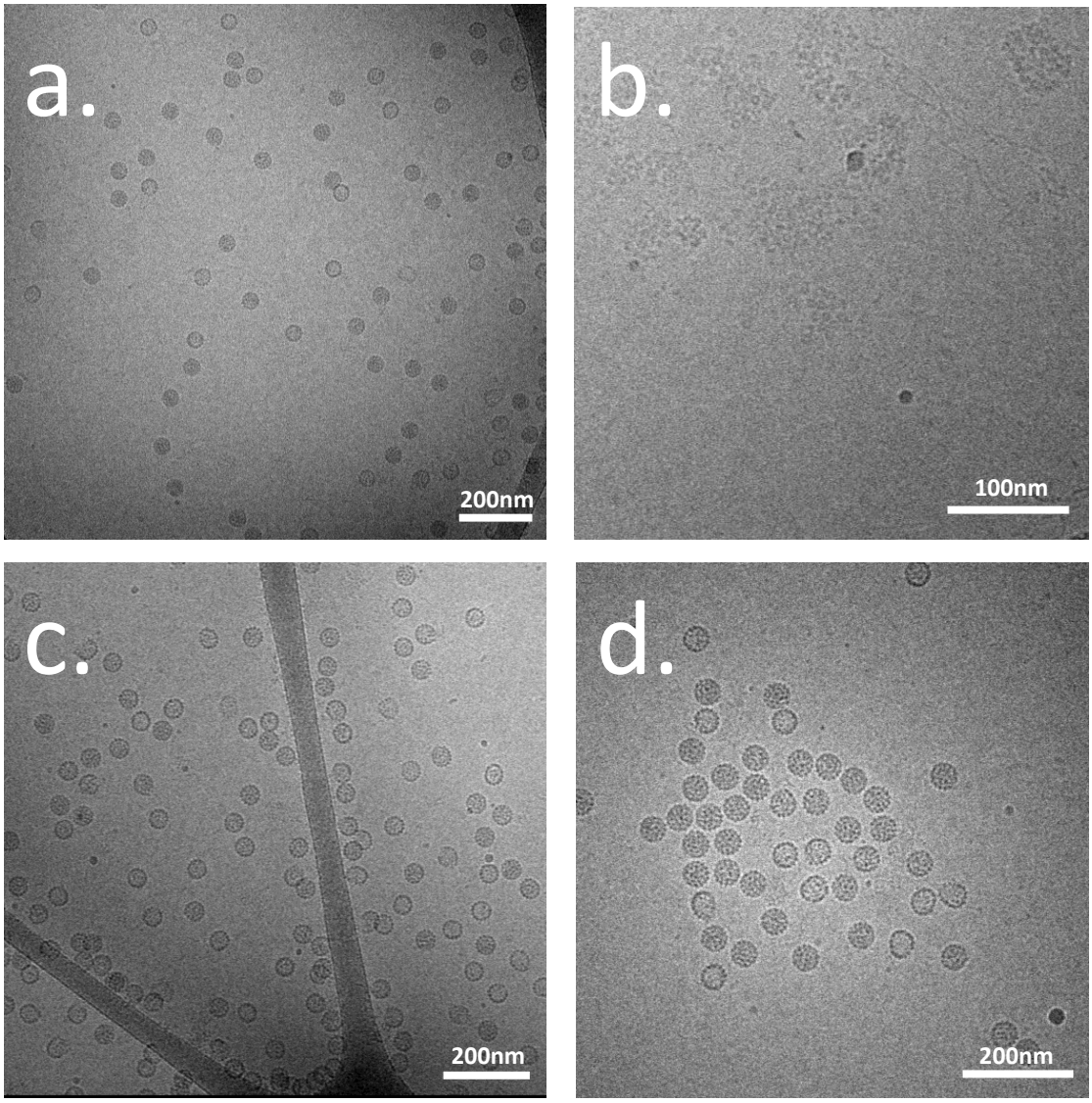

Figure S7: Additional cryo-TEM images of $\sim 0.4^{\mathrm{mg}}/_{\mathrm{mL}}$ wtSV40 at pH 10.7 in 150 mM NaCl and 50 mM CAPS buffer.

6 SAXS model of wtSV40 at pH 10.7 using 50 mM CAPS buffer

To model the partially empty wtSV40 in the CAPS buffer at pH 10.7, we have used the following scaling approximation to the contribution of the excesses electron density of the different components:

$$I(q \approx 0) \propto \delta^2_{\text{empty}} = \left(\delta_{\text{capsid}} + \delta_{\text{inner sphere}}\right)^2 + \delta^2_{\text{dsDNA}} \approx \left(\delta_{\text{capsid}} + \delta_{\text{inner sphere}}\right)^2 \tag{S3}$$

where δ is the contribution to the scattering intensity at low angles from the different structural components owing to the excesses electron density contribution. δ is proportional to $\Delta\rho \cdot V$. In our case, the scattering intensity of the empty particle originates from the capsid shell, the inner sphere that represents the histones and VP2/3 that were left inside the capsid after the dsDNA escaped, and the dsDNA that was outside the particle. We estimated the volumes and number of electrons of the different component using D+ software[7] (https://scholars.huji.ac.il/uriraviv/book/d-0) and found that $\frac{\delta^2_{\text{dsDNA}}}{\left(\delta_{\text{capsid}}+\delta_{\text{inner sphere}}\right)^2} \approx 0.06$.

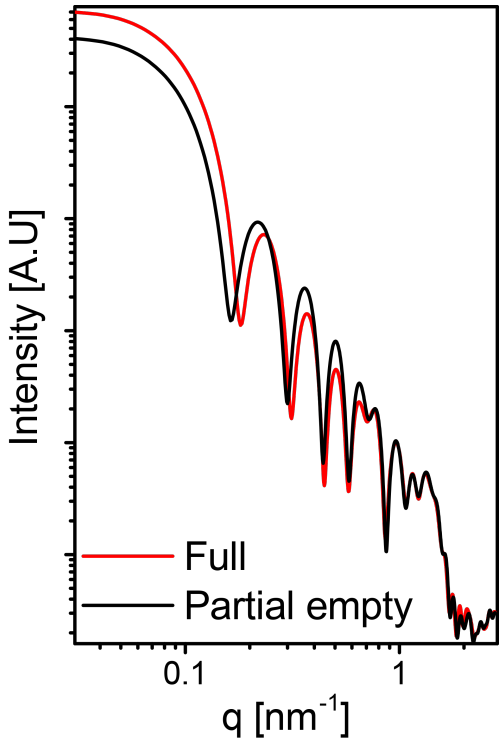

Figure S8: Comparison between the expected scattering intensity of full wtSV40 particle and a partially empty particle. The intensity at the lowest q range is lower for the partially empty particle as its total mass is lower. Additionally, the first two oscillations are shifted towards lower scattering angles owing to the reduced contribution from the inner electron density. The positions of the oscillations at higher q values remained unchanged.

7 Reversibility and infectivity measurements of wtSV40 virus at different pH values

At pH 10, both empty, full, and deformed capsids appeared (Figure 3, S1, and S2). At pH 3, the particles deformed and aggregated (Figure 3 and S1). The wtSV40 structural reversibility after incubation at pH 3 or 10 was measured by both SAXS and cryo-TEM (Figure S9). The infectivity of the virus after incubation at pH 3 or 10 was also checked using the FACS method (Figure S10), based on which the titer was calculated (Figure S11).

Titration protocol was performed as was previously described[8]. SV40 at capsid protein concentration of $\sim$0.05 $^{\mathrm{mg}}/_{\mathrm{mL}}$ were first incubated for 90 min at pH 3,7, or 10 using 50 mM of the relevant buffer (see Table S3). Following the initial incubation, SV40 solutions were dialyzed for 1h against a solution containing 150 mM NaCl and 50 mM MOPS at pH 7. The dialyzed solutions were initially diluted at a ratio of 1:50, using serum free Dulbecco's Modified Eagle Medium (DMEM, Biological Industries), and then by a series of five two-fold dilutions, where the final dilution ratio was $1:1{,}600$. CV1 cells were then infected by the serial dilutions for 1 h at 37 °C in DMEM, and then incubated in DMEM supplemented with 10% Feta bovine serum (FBS) at 37 °C for $48\,\mathrm{h}$. The cells were then harvested, fixed, and stained for SV40 T-antigen, encoded by the virus using α-Tag (Pab416) antibody (#ab16879) at a ratio of $1:100$ in $5\,\mathrm{wt}\%$ bovine serum albumin (BSA) in PBS (pH = 7.4), followed by a secondary antibody, $\alpha-$mouse-IgG-Daylight488 (#ab98794) at a ratio of $1:200$ in $5\,\mathrm{wt}\%$ BSA in PBS (pH = 7.4). The percentage of infected cells was quantified by flow cytometry, with a gating based on mock-infected cells. The fluorescence intensity of the stained cells was measured by the fluorescence-activated cell sorting (FACS) and analysis was done using Kaluza (Beckman coulter) software (Figure S10). The titer, Ti was calculated according to FACS results (Figure S11), where

$$Ti = \frac{N_{\text{CTI}} \times f_{IC}}{V_{IV}},$$

N_{CTI} is the number of cells at the time of infections (1.38×10^6), F_{IC} is the fraction of T-ag positive cells, and V_{IV} is the volume of the virus at each dilution (mL). The average titer of the original virus stock at each pH was calculated using three data points as shown Figure S11.

SV40 titers were $1.28 \pm 0.04 \times 10^6$, $2.80 \pm 0.15 \times 10^6$, and $6.51 \pm 0.16 \times 10^5$ cells$\cdot\mu\text{L}^{-1}$ for virus that was incubated at pH 3, 7, and 10 prior to infection, respectively. Taking the titer of SV40 that was incubated at pH 7 as a reference, the titers results showed that viruses incubated at pH 3, maintained part of their infectivity level, with a T-antigen expression ratio of $45.7 \pm 1.4\%$ compared with the reference sample, kept under physiological conditions (Figure S10b and S11). This experiment may provide insight into the ability of wtSV40 to pass through the acidic endosomal pH environment and remain infective[9,10]. Following incubation at pH 10, however, the infectivity was only $23.2 \pm 0.6\%$ of the reference sample (Figure S10d and S11). The results are in agreement with earlier observations[10].

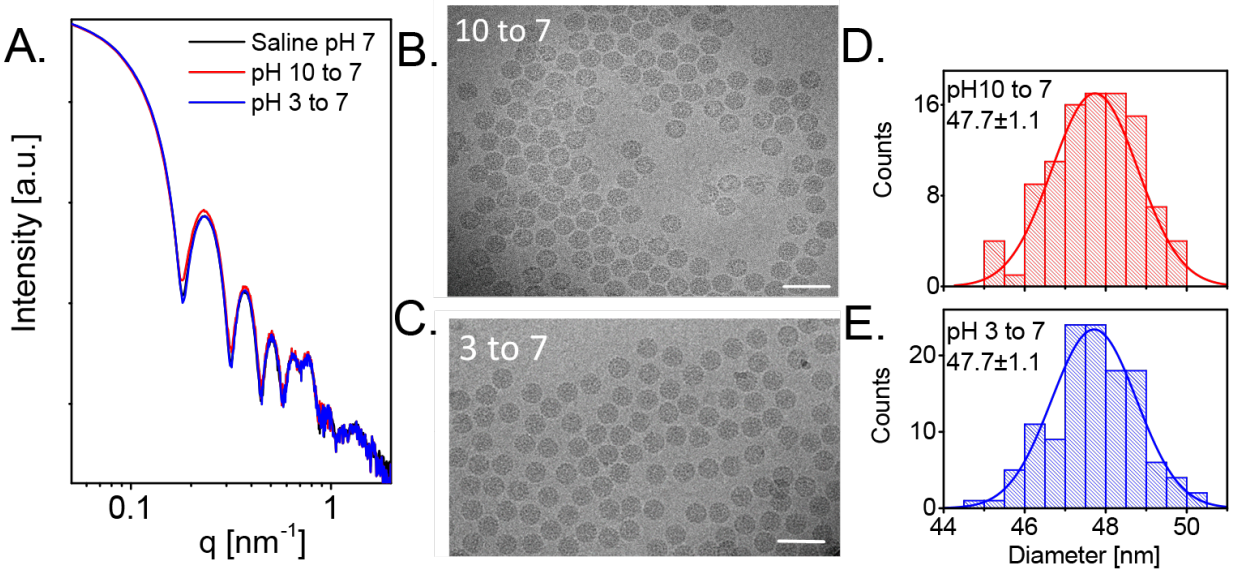

Figure S9: Reversibility analysis. **A.** Azimuthally-integrated background-subtracted SAXS curves from wtSV40 in saline at pH 7 (black curve), and wtSV40 that was incubated for 1.5 h in 150 mM NaCl at pH 10 or 3 and then dialyzed against 150 mM NaCl at pH 7 (dotted red and blue curves, respectively). Date were measured at P12 EMBL BioSAXS Beamline in PETRA III (DESY, Hamburg). **B.** Cryo-TEM image of wtSV40 that was incubated for 1.5 h in 150 mM NaCl at pH 10 and then dialyzed against 150 mM NaCl at pH 7. **C.** Cryo-TEM image of wtSV40 that was incubated for 1.5 h in 150 mM NaCl at pH 3 and then dialyzed against 150 mM NaCl at pH 7. **D.** Histogram of particles diameter in *B*. **E.** Histogram of particles diameter in *C*. Scale bars are 100 nm.

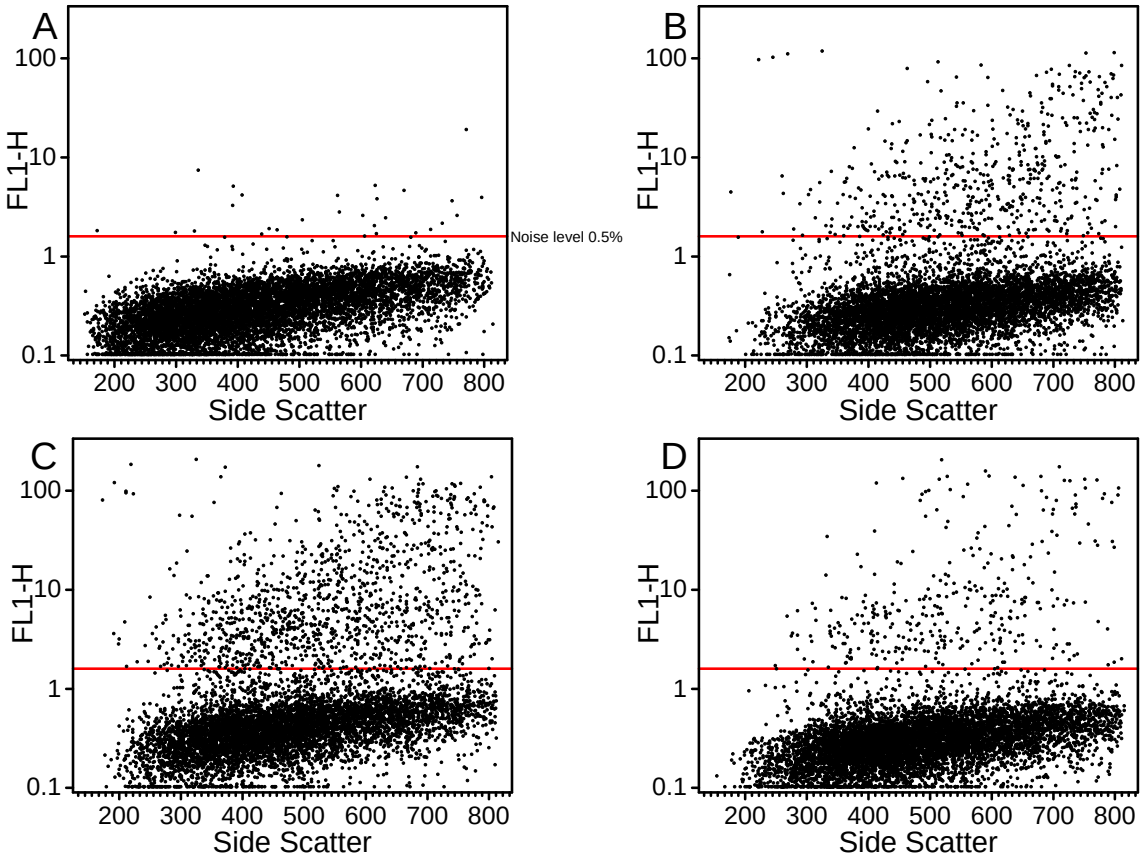

Figure S10: Example of FACS data of infected CV1 cells using the highest concentration of SV40 (obtained after the initial 50-fold dilution). FACS results of uninfected cells (A.), Cells that were infected by SV40 after incubating for 90 min at pH 3 (B.), pH 7 (C.) and pH 10 (D.). The red line marks the border between the uninfected cell and few dots which we consider as noise level, neasured to be 0.5%, determined by the control experiment in (A.)

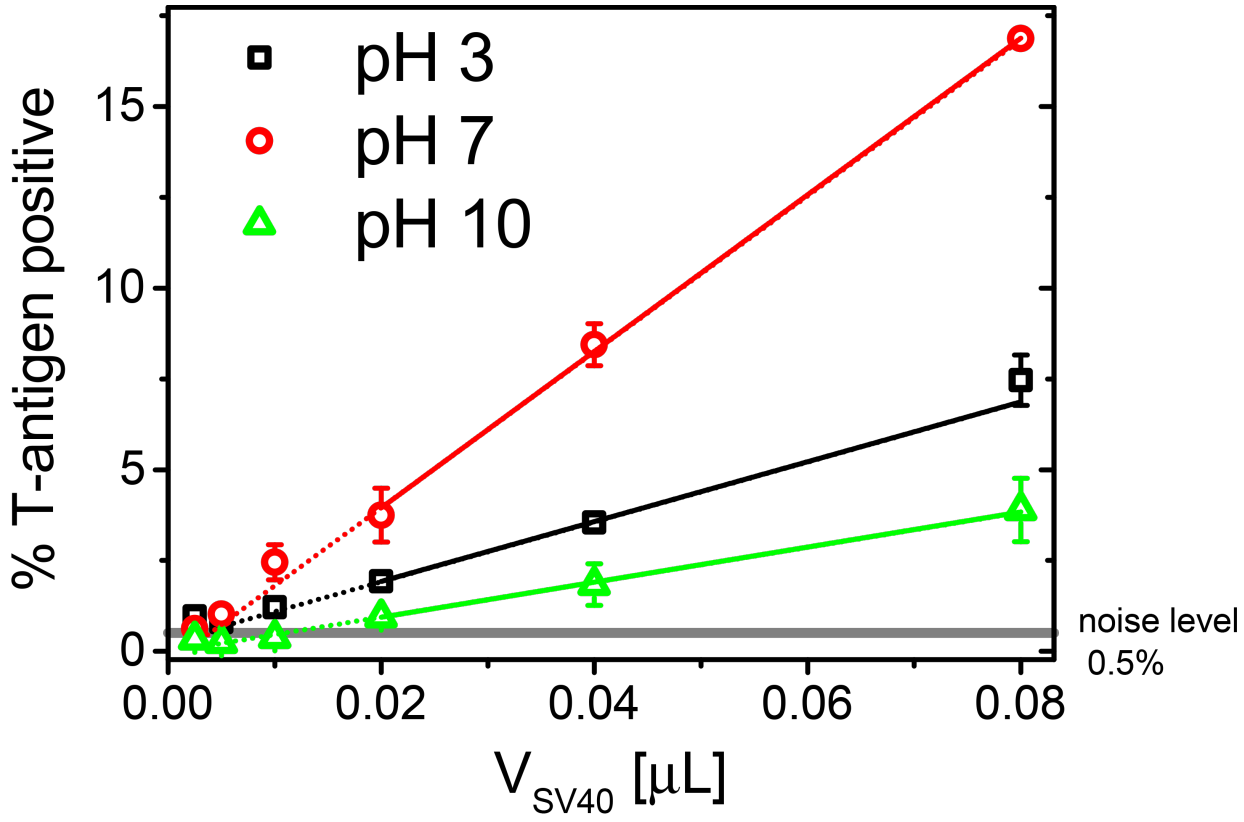

Figure S11: Titration curves. Percentage of infected cells (measured as T-antigen-positive cells) as a function of the volume of the initial SV40 stock solution, used for infection. The initial SV40 solutions were incubated for 1 h at the indicated pH values prior to infection (see Experimental Section). The data points at the lowest three stock solution volumes were not used to calculate the titers because their infection level was close to the noise level, marked by the gray line. The titers were obtained from the slopes of the solid lines that were fitted to the three highest volumes at each pH. The dotted lines were extrapolated from the solid lines and only serve as a guide to the eye.

8 Additional time-resolved cryo-TEM images

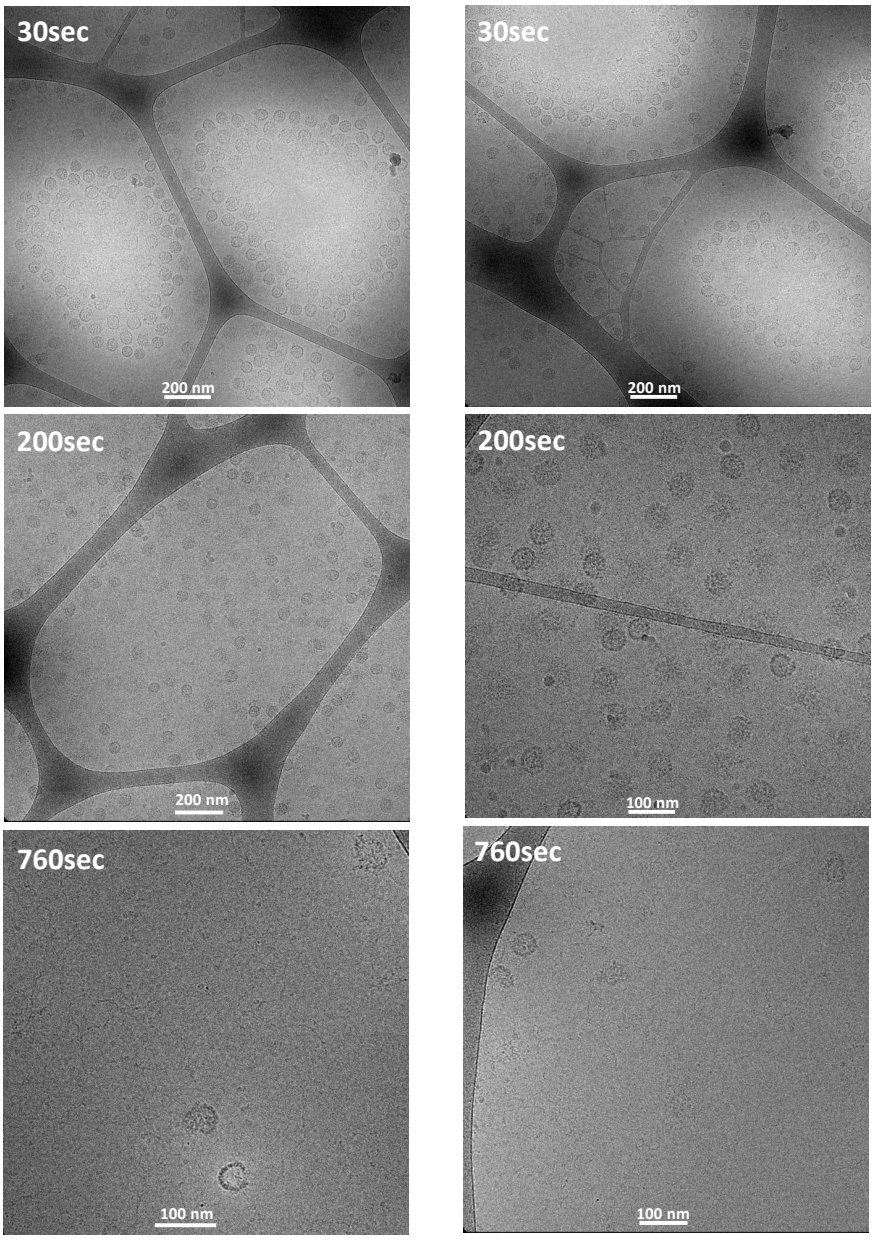

Figure S12: Additional time-resolved cryo-TEM images of wtSV40 at pH 10.7, using the carbonate buffer. The times elapsed after mixing the virus particles with the carbonate buffer are indicated in the figures.

9 The late phases of the disassembly process

Following the escape of the dsDNA at pH 10.7 (using the carbonate buffer), the virus particles disassembled. Our SAXS results suggest that the disassembly process passed through a partially disassembled state, at which the SAXS curve contained weakly oscillating signals (such as the blue curve in Figure S13). In this state, the solution, most likely, contained capsid fragments of different sizes, which contributed to the total scattering intensity and the relatively high average mass (given by $I\left(q \rightarrow 0\right)$). At later time points, the SAXS signals had significantly lower $I\left(q \rightarrow 0\right)$ and hence much lower average masses. Furthermore, the lack of oscillations suggests that on average, the capsid almost completely disassembled (orange signal in Figure S13). As the solution in these two states was extremely polydispersed (containing different components such as capsid proteins, histones, circular dsDNA and their assemblies) modeling was too complicated. Instead, we used the measured intensity curves as additional states for modeling the rest of the disassembly kinetic time-resolved SAXS (TR-SAXS) signals.

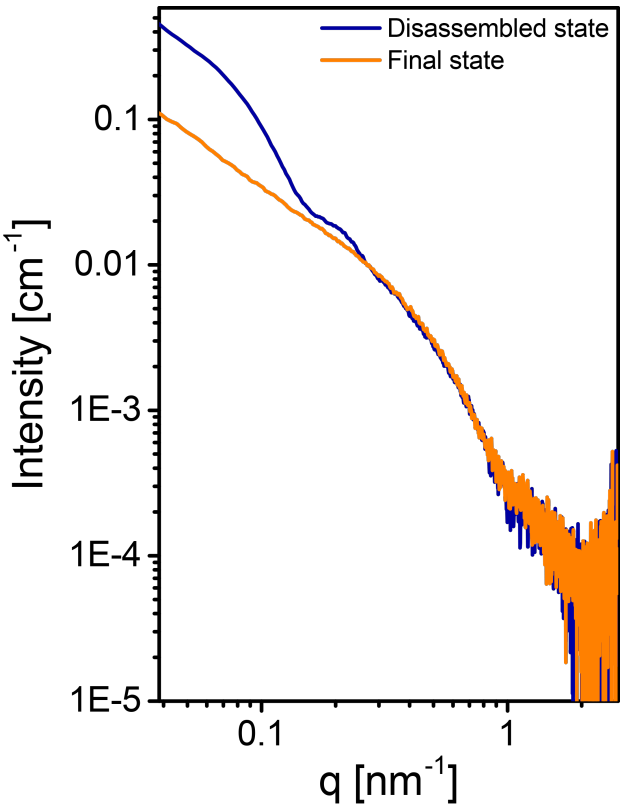

Figure S13: Measured scattering intensity curves during the disassembly process, used for modeling the final two phases of the disassembly. The orange curve corresponds to the end of the disassembly process, where the virus almost completely disassembled. The blue curve (Disassembled state) corresponds to the state of the solution at the end of phase **III**, where the solution contained fragments of capsid and minichromosome. Date were meassured at ID02 beamline in ESRF, Grenoble.

10 Using hybrid models to analyze the SAXS curves from wtSV40, swollen wtSV40, and partially empty wtSV40

During the initial two phases of the disassembly process our TR-SAXS and time-resolved cryo-TEM measurements suggest that the disassembly path was dominated by two intermediate states; a swollen SV40, and a partially empty capsid, following the escape of the circular dsDNA. To model the different states, we used our home developed software, D+,[7,11] that can calculate the expected scattering intensities from hybrid models containing both atomically and geometrically modeled

subunits.

High resolution models - Hybrid models

To improve the resolution of our models, we used the crystallographic atomic model of the capsid shell[12,13], our hydration layer algorithm[7] to take into account the contribution from the hydration layer around the atomic capsid model, and a uniform sphere model to account for the contribution of the inner, rather disordered and dynamic, minichromosome. This type of model combined elements from both atomic and low resolution information, hence we shall refer to it as a hybrid model. To calculate the expected scattering intensity of the hybrid model we used our home developed software D+ (https://scholars.huji.ac.il/uriraviv/book/d-0)[7,11]. We computed the scattering from the atomic model of the capsid, based on protein data bank (PDB) entry 1SVA[12]. The total scattering amplitude of the wtSV40 is given by,

$$F\left(\vec{q}\right) = F^{\text{sol}}_{\text{capsid}}\left(\vec{q}; f_r\right) + F_{\text{hydration}}\left(\vec{q}\right) + F_{\text{Inner sphere}}\left(\vec{q}; r_{\text{inner}}\right). \tag{S4}$$

$F^{\text{sol}}_{\text{capsid}}\left(\vec{q}; f_r\right)$ is the scattering amplitude of the solvated atomic structure of the capsid. f_r is a scaling factor, multiplying all the vectors of the pentamer geometric centers, thereby accounting for small uniform deviations in the size of the capsid from its crystal structure. $F_{\text{hydration}}\left(\vec{q}\right)$ is the scattering amplitude from the hydration layer around the capsid and $F_{\text{Inner sphere}}\left(\vec{q}; r_{\text{inner}}\right)$ is the approximation to the scattering contribution from the minichromosome modeled as a uniform sphere with radius, r_{inner}. The scattering intensity is then given by,

$$I\left(q\right) = \frac{1}{4\pi}\int_{\Omega_q} F\left(\vec{q}\right) F^{*}\left(\vec{q}\right) d\Omega_q \tag{S5}$$

where, $I\left(q\right)$ is the orientation-averaged scattering intensity in solution and Ω_q is the reciprocal-space solid angle. The hybrid model parameters for wtSV40 and partially empty particles were calibrated by fitting the model to the experimental data in Figure 4b. and c. The swollen configura-

tion of the virus was determined by finding the best fitted f_r parameter to a two-state disassembly kinetics (dominated by wtSV40 and swollen SV40), measured in the stopped-flow setup (Figure 5a and section 11 in SI). All fitting parameters can be found in Table S2 and Figure S14.

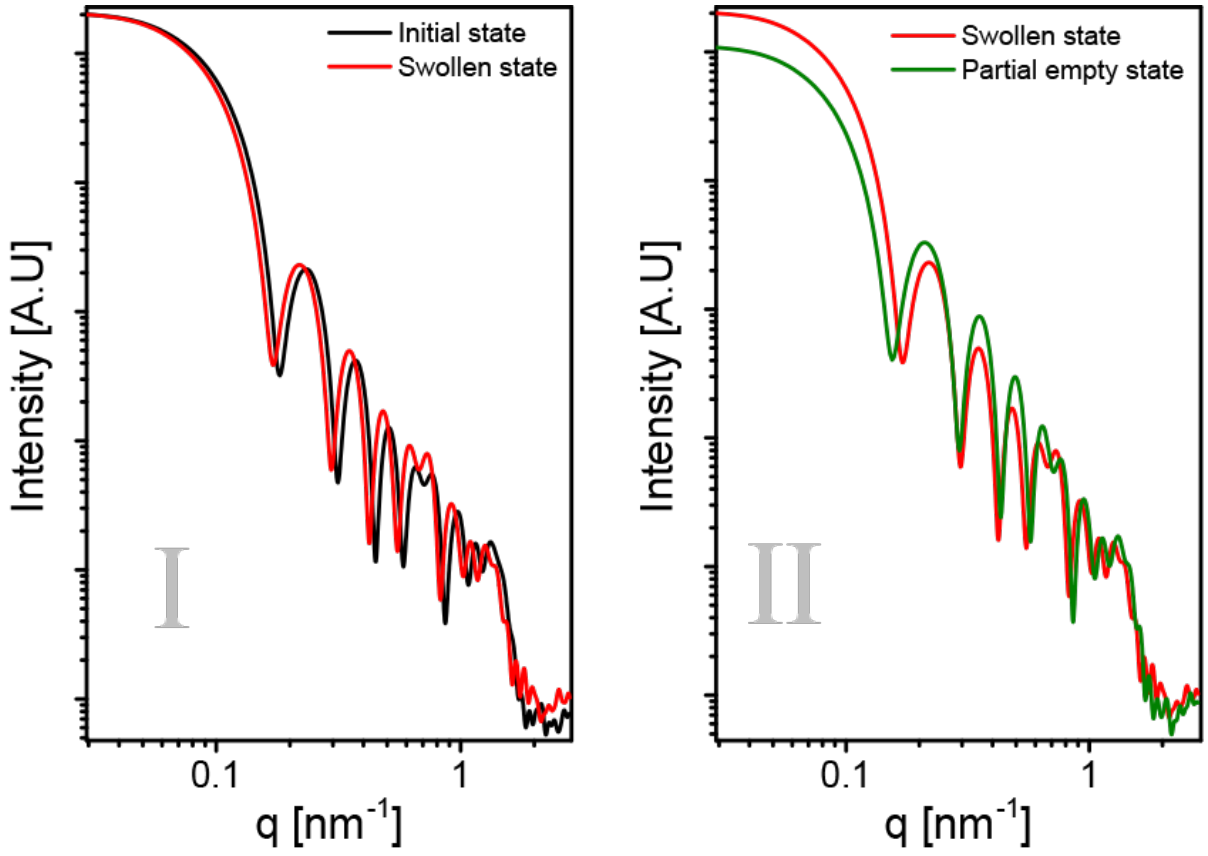

Figure S14: Calculated scattering intensities of the initial structure of wtSV40 and dominant intermediate states in the first two phases of disassembly process. At phase **I** (swelling phase) the two models required to fit the scattering data were the initial wtSV40 structure (calibrated by the static measurements at saline solution) and the swollen SV40 state that was found by minimizing Equation S6 in the main text. During phase **II**, the scattering curves were dominated by the swollen SV40 state and the partially empty SV40 state (the state of the virus following the escape of the circular dsDNA).

Table S2: The best fitted model parameters of the three amplitudes used in Equation S4.

Model	f_r	Hydration layer thickness [nm]	$\Delta\rho$ of Hydration layer [e/nm^3]	$\Delta\rho$ of Inner sphere [e/nm^3]	r_{inner}
wtSV40	1.0125	0.28	30	44.5	18.8
Swollen SV40	1.07	0.28	30	39	19.5
Partially empty SV40	1.03	0.28	30	12	19

11 Analysis of the time-resolved SAXS data

Fitting the swelling phase, presented in Figure 7a. (phase **I**) was performed by considering the swelling process as a two state first order reaction, described by a single rate constant parameter, [Initial] $\xrightarrow{k}$ [Swollen]. The data matrix $\mathbf{D}$ was fitted to the kinetic model matrix, $\mathbf{M}(k)$, by minimizing the χ^2 function given by,

$$\chi^2 = \sum_{t_i=t_1}^{t_n} \sum_{q_j=q_1}^{q_N} \left(\frac{\mathbf{M}(k)_{q_j,t_i} - \mathbf{D}_{q_j,t_i}}{\sigma_{q_j,t_i}} \right)^2 \tag{S6}$$

where $\mathbf{D}_{q_j,t_i}$ is the measured average scattering intensity at q_j and at time t_i following the mixing phase, σ_{q_j,t_i} is the standard deviation of the measured average intensity and $I_{\text{model}}(q_j, t_i)$ is the modeled matrix $\mathbf{M}(k)_{q_j,t_i}$ at q_j and t_i, given by:

$$\begin{aligned} \mathbf{M}(k)_{q_j,t_i} = M_0 \cdot \exp(-kt_i) \cdot I_{\text{initial}}(q_j) + \\ M_0 \cdot (1 - \exp(-kt_i)) \cdot I_{\text{swollen}}(q_j) \end{aligned} \tag{S7}$$

with $I_{\text{initial}}(q_j)$ and $I_{\text{swollen}}(q_j)$ the models of the wtSV40 and the swollen conformation, respectively, and M_0 is the initial mass fraction of particles that was set to 1.

Fitting the slow kinetic phases measured with the flow-cell setup shown in Figure 7 (phases **II–IV**) was done by solving for each measured time point, t_i, the non-negative least square problem[14], $\underset{x}{\mathbf{min}} \| (\mathbf{M}\mathbf{x}(t_i) - \mathbf{I}_{\text{signal}}(t_i)) \cdot \mathbf{w} \|_2^2$, where $\mathbf{M}$ is a $q_N \times 5$ matrix containing in each column one of the 5 modeled principle states, where $\mathbf{x}(t_i)$ is a 5×1 vector containing non-negative values for the mass fraction of each principle state at time t_i, $\mathbf{I}_{\text{signal}}(t_i)$ is the measured signal at time t_i and $\mathbf{w}$ is a $q_N \times 1$ vector that weights the intensities at each q value by $1/\sigma_{q_j}$. Full fitting results and the model for each state are shown in Figure 7 and Sections 6,10 and 11 in the SI.

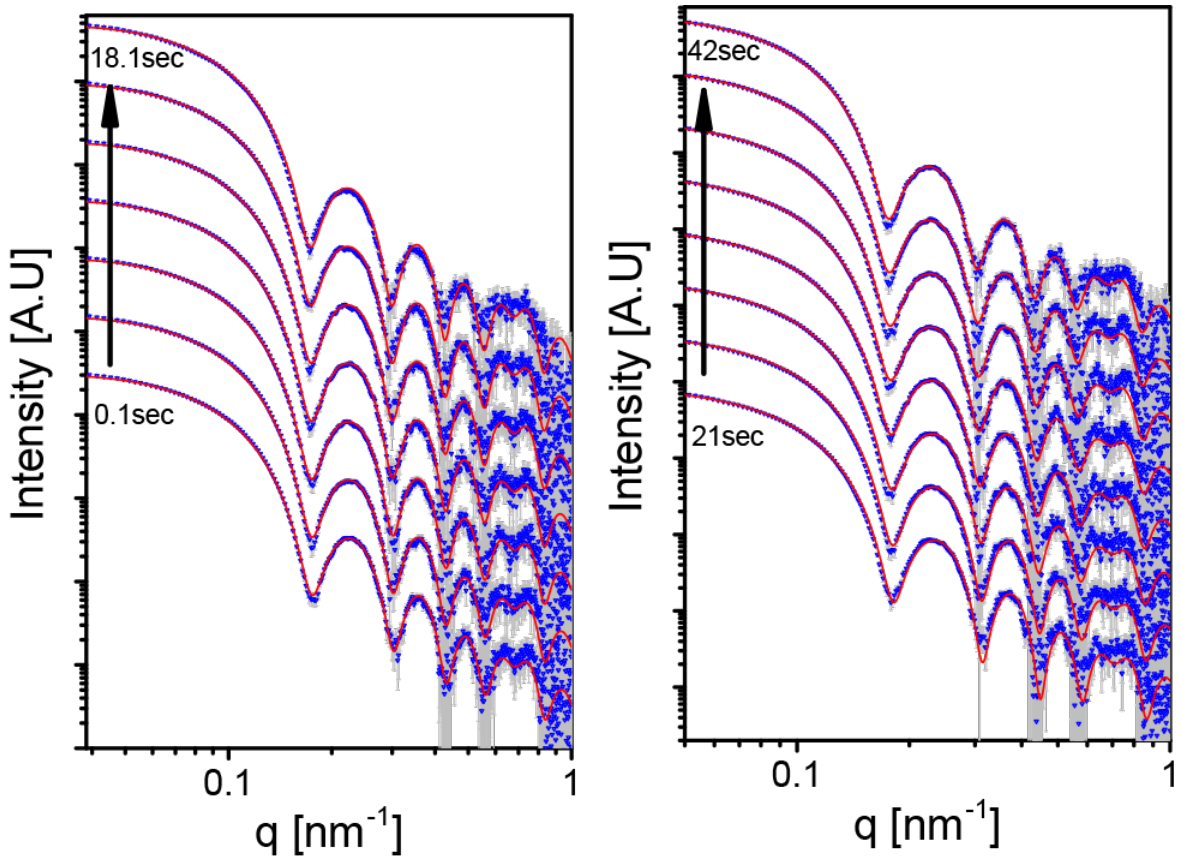

Figure S15: The results of the fitting (red curves) to the TR-SAXS data (blue symbols and gray error bars) of the swelling phase during the first 42 sec of disassembly at pH 10.7 (using the carbonate buffer). Selected time points are shown in Figure 5a and 7. Measurements were performed at ID02 beamline in ESRF, using the stopped-flow setup. The times elapsed after mixing the virus particles with the carbonate buffer are indicated in the figure. The interval between consecutive measurements was 3 sec. The curves were shifted for clarity of presentation.

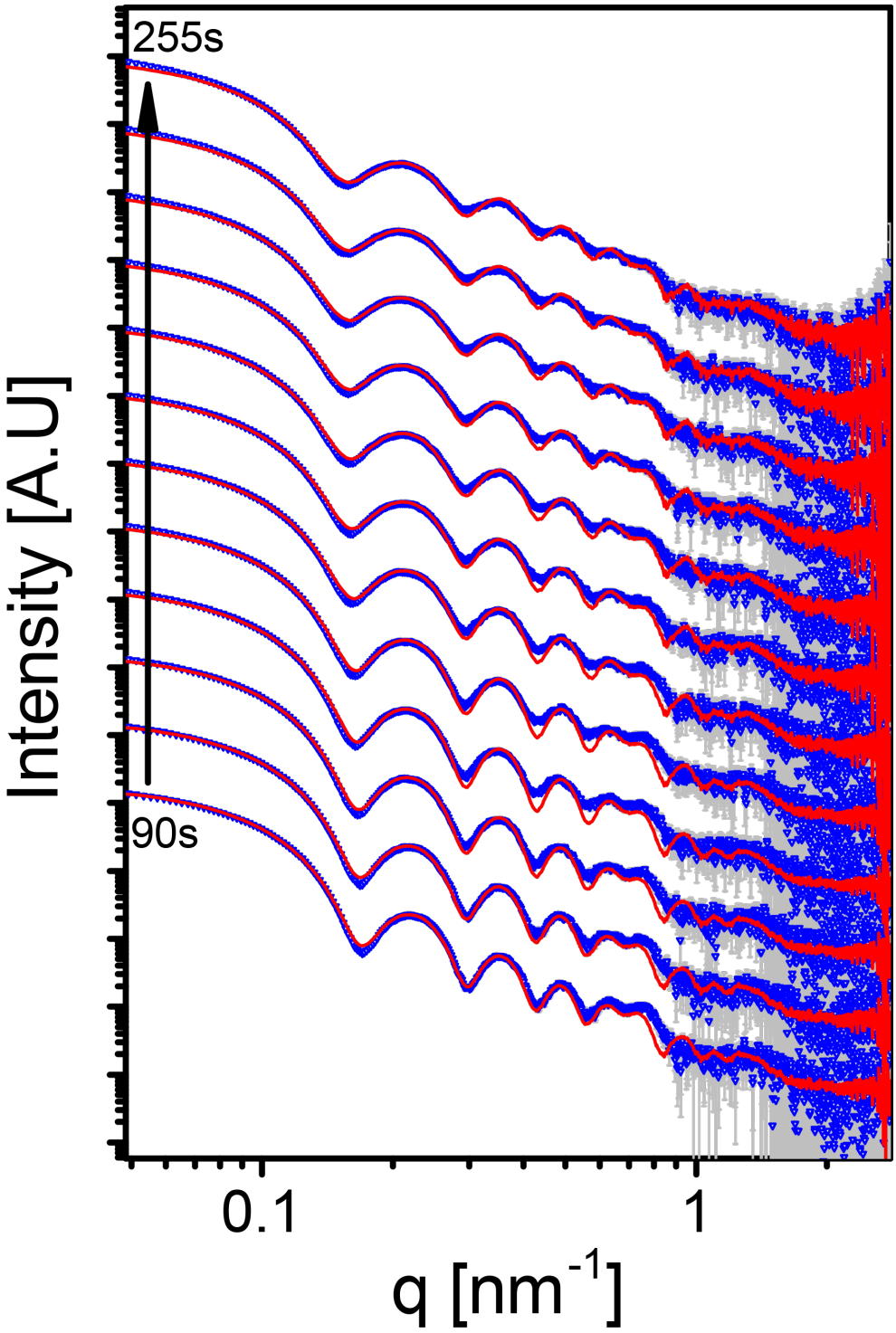

Figure S16: The results of the fitting (red curves) to the TR-SAXS data (blue symbols and gray error bars) of the second phase of the disassembly reaction at pH 10.7 (using the carbonate buffer). Selected time points are shown in Figure 5b and 7. Measurements were performed in the flow-through setup at ID02 beamline in ESRF. The times elapsed after mixing the virus particles with the carbonate buffer are indicated in the figure. The interval between consecutive measurements was 15 sec. The curves were shifted for clarity of presentation.

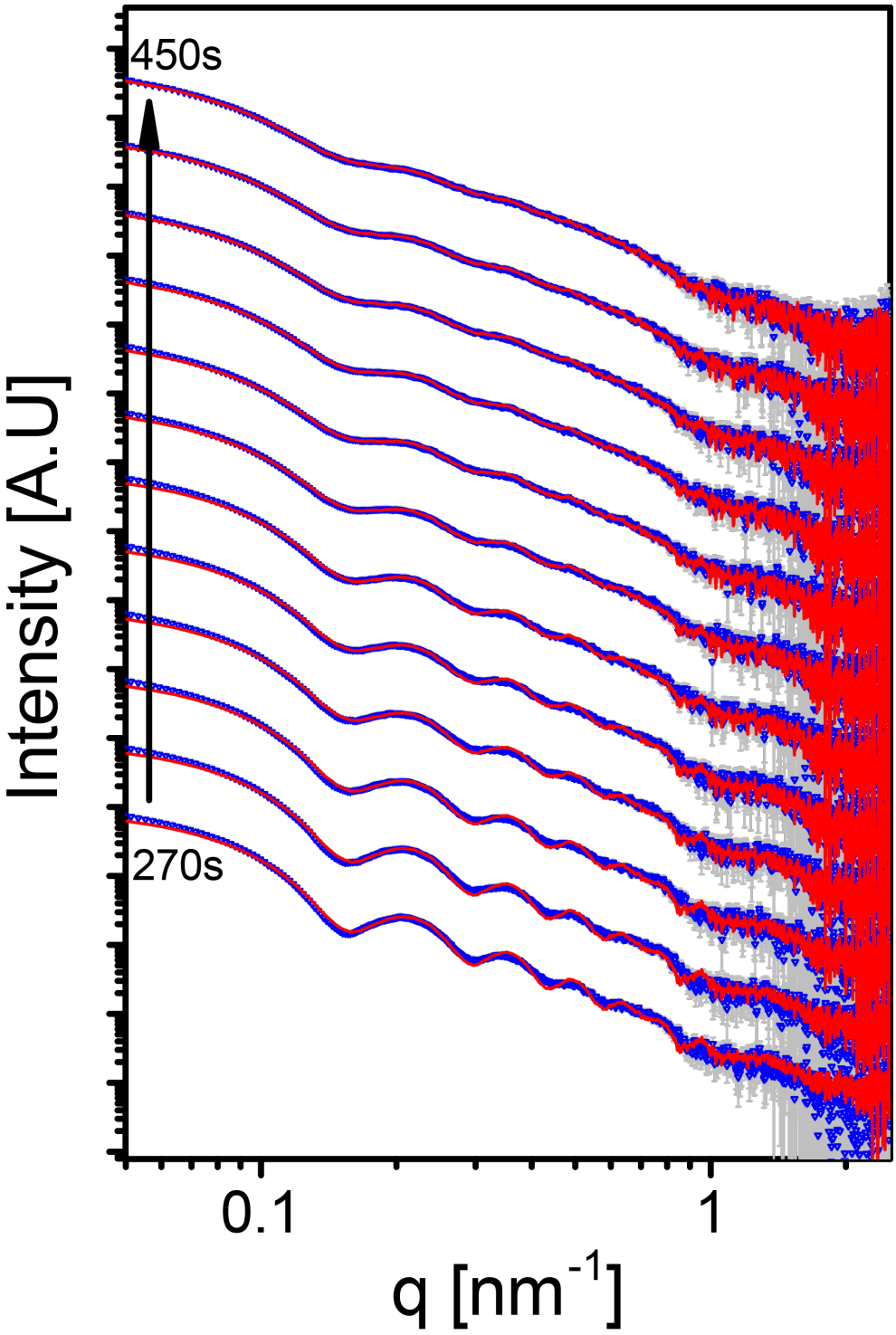

Figure S17: The results of the fitting (red curves) to the TR-SAXS data (blue symbols and gray error bars) of the third phase of the disassembly reaction at pH 10.7 (using the carbonate buffer). Selected time points are shown in Figure 5c and 7. Measurements were performed in the flow-through setup at ID02 beamline in ESRF. The times elapsed after mixing the virus particles with the carbonate buffer are indicated in the figure. The interval between consecutive measurements was 15 sec. The curves were shifted for clarity of presentation.

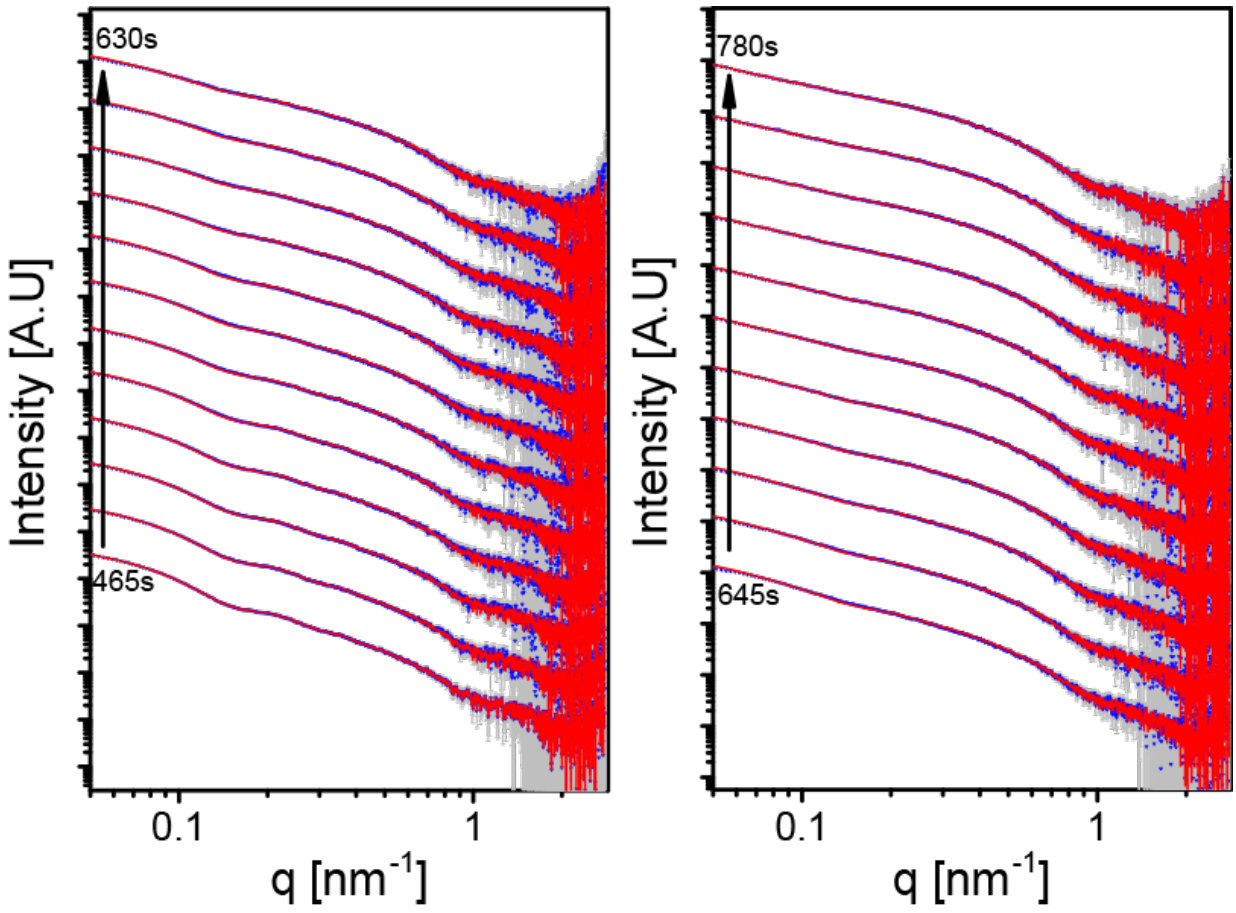

Figure S18: The results of the fitting (red curves) to the TR-SAXS data (blue symbols and gray error bars) of the fourth phase of the disassembly reaction at pH 10.7 (using the carbonate buffer). Selected time points are shown in Figure 5d and 7. Measurements were performed in the flow-through setup at ID02 beamline in ESRF. The times elapsed after mixing the virus particles with the carbonate buffer are indicated in the figure. The interval between consecutive measurements was 15 sec. The curves were shifted for clarity of presentation.

12 The buffers used at each of the pH values

Table S3 provides a list of the buffers used at each pH value. Citric acid/Citrate and Carbonate/Bicarbonate buffers were prepared by mixing stock solutions of the acid and conjugated base to the volume and pH values needed. 2-(N-morpholino)ethanesulfonic acid (MES), 3-morpholinopropane-1-sulfonic acid (MOPS), 2-Amino-2-hydroxymethyl-propane-1,3-diol (TRIS), and N-cyclohexyl-3-aminopropanesulfonic acid (CAPS) were made by dissolving the buffer and adjusting the pH using either 37% HCl or $10\,\mathrm{M}$ NaOH solutions, according to the starting pH value of the buffer. All buffer concentrations were $0.5\,\mathrm{M}$, unless otherwise indicated.

Table S3: List of Buffers used in the experiments

pH	Buffer
3	Citric acid/citrate
4	Citric acid/citrate
5.5	MES
7.2	MOPS
8	TRIZMA-Base
9	TRIZMA-Base
10	Carbonate/bicarbonate
10.7	Carbonate/bicarbonate
10.7	CAPS ($0.4\,\mathrm{M}$)

References

[1] G. Saper, S. Kler, R. Asor, A. Oppenheim, U. Raviv and D. Harries, *Nuc. Acid. Res.*, 2012, **41**, 1569–1580.

[2] R. Asor, O. Ben-nun Shaul, A. Oppenheim and U. Raviv, *ACS Nano*, 2017, **11**, 9814–9824.

[3] R. Asor, D. Khaykelson, O. Ben-nun Shaul, A. Oppenheim and U. Raviv, *ACS Omega*, 2019, **4**, 58–64.

[4] T. Ben-Nun, A. Ginsburg, P. Székely and U. Raviv, *J. Appl. Cryst.*, 2010, **43**, 1522–1531.

[5] P. Székely, A. Ginsburg, T. Ben-Nun and U. Raviv, *Langmuir*, 2010, **26**, 13110–13129.

[6] T. Ben-Nun, R. Asor, A. Ginsburg and U. Raviv, *Isr. J. Chem.*, 2015.

[7] A. Ginsburg, T. Ben-Nun, R. Asor, A. Shemesh, L. Fink, R. Tekoah, Y. Levartovsky, D. Khaykelson, R. Dharan, A. Fellig and U. Raviv, *Journal of Applied Crystallography*, 2019, **52**, 219–242.

[8] N. Drayman and A. Oppenheim, *Current protocols in cell biology*, 2011, **51**, 26–11.

[9] A. Ashok and W. J. Atwood, *Journal of virology*, 2003, **77**, 1347–1356.

[10] S. Engel, T. Heger, R. Mancini, F. Herzog, J. Kartenbeck, A. Hayer and A. Helenius, *Journal of Virology*, 2011, **85**, 4198–4211.

[11] A. Ginsburg, T. Ben-Nun, R. Asor, A. Shemesh, I. Ringel and U. Raviv, *Journal of Chemical Information and Modeling*, 2016, **56**, 1518–1527.

[12] T. Stehle, S. J. Gamblin, Y. Yan and S. C. Harrison, *Structure*, 1996, **4**, 165–182.

[13] T. Stehle, Y. Yan, T. L. Benjamin and S. C. Harrison, *Nature*, 1994, **369**, 160.

[14] C. L. Lawson and R. J. Hanson, *Solving least squares problems*, Siam, 1995, vol. 15.